Clinical Spectroscopy 3 (2021) 100011

Contents lists available at ScienceDirect

Clinical Spectroscopy

journal homepage: www.elsevier.com/locate/clispe

# Hyperspectral characterization of the MSTO-211H cell spheroid model: A FPA–FTIR imaging approach

Valentina Notarstefano [a,*], Simona Sabbatini [b], Maurizio Sabbatini [c], Aldo Arrais [c], Alessia Belloni [a], Chiara Pro [a], Lisa Vaccari [d], Domenico Osella [c], Elisabetta Giorgini [a]

[a] Department of Life and Environmental Sciences, Università Politecnica delle Marche, Via Brecce Bianche, 60131, Ancona, Italy
[b] Department of Materials, Environmental Sciences and Urban Planning, Università Politecnica delle Marche, Via Brecce Bianche, 60131, Ancona, Italy
[c] Dipartimento di Scienze e Innovazione Tecnologica, Università del Piemonte Orientale, Viale Michel 11, 15121, Alessandria, Italy
[d] SISSI Beamline, Elettra-Sincrotrone Trieste, S.C.p.A., S.S. 14 – Km 163.5, 34149, Basovizza, Trieste, Italy

ARTICLE INFO

*Keywords:*
FPA-FTIRI
Hyperspectral analysis
3D spheroids
Malignant pleural mesothelioma
Cisplatin
MSTO-211H

ABSTRACT

Multicellular spheroids are the new frontier for studying how the tumour micro-environment interferes with drug uptake and response, since they can reproduce a three-dimensional cellular organisation mimicking the behaviour of *in vivo* solid tissues. In this study, we exploited Focal Plane Array - Fourier Transform Infrared Imaging spectroscopy to characterize the biochemical features, in terms of distribution and composition of the meaningful macromolecules (lipids, proteins, sugars and nucleic acids), of malignant pleural mesothelioma spheroid sections, and, as further extent, to investigate the penetrating effects of cisplatin within the spheroid mass. The hyperspectral imaging analysis evidenced, in untreated spheroids, the occurrence of a replicative outer region and a hypoxic inner one, as suggested by the band area ratios related to lipid alkyl chains (2925/2960) and glycogen (1020/1650), which showed the highest values in the inner region. Moreover, the HCA spectroscopic images showed, after cisplatin treatment, an increase of the band area ratio related to lipid carbonyl ester moiety (1740/2925), suggesting the occurrence of lipid peroxidation; furthermore, the band area ratio related to nucleic acids (1240/1220) revealed a DNA fragmentation along all regions of spheroids that may be related to apoptotic mechanisms, whereas a reduction of the band area ratios related to glycogen and carbohydrates (1020/1650 and 1054/1650, respectively) appeared consistent with an inhibition of cell division. The few spectral differences between the outer and the inner regions of cisplatin-treated spheroids pointed out the diffuse penetrating effect of the drug.

## Introduction

Investigation of solid tumors, both in terms of biomolecular composition and drug-uptake mechanisms, remains a major problem, due to significant limitations in reproducing the complexity and pathophysiology of *in vivo* tumor tissues [1,2]. Furthermore, animal-based models, which could better reproduce the tumor behavior, are limited by ethical concerns and do not allow high-throughput screenings [3]. In this light, a new experimental model of cell aggregation in culture is represented by spheroids, cellular aggregates obtained by several cellular types [4], which reproduce a three-dimensional cellular organisation mimicking the behaviour of *in vivo* solid tissues [5,6]. The deepening of their biochemical structure and mechanisms, appear mandatory for better understanding how the tumour micro-environment interferes with drug uptake and response [7,8]. Mesothelioma spheroids can be considered a strategic tool to investigate both the tumour mass behaviour and the effects of chemotherapy drugs, due to this tumour shows high aggressiveness and resistance to stimuli inducing reduction or stasis of tumour mass [9].

Since several properties of spheroids are attributable to their own architecture, the application of a methodological investigation which let conserve the structural integrity, such as Focal Plane Array–Fourier Transform Infrared Imaging (FPA-FTIRI) spectroscopy, has become of crucial importance. FPA-FTIR let acquire, at the same time and on the same sample, in a rapid and non-destructive way, multiple mid-infrared spectra, giving the biomolecular fingerprint of the sample and highlighting subtle molecular changes not detectable by optical microscopy [10,11].

At the best of our knowledge, there is only a study in which FPA-FTIRI has been applied to investigate colon DLD-1 cell spheroids [4]. Srisongkram et al. analysed melanoma 3D cell cultures by FTIR Microspectroscopy, but cells were trypsinised before spectral acquisition, losing any information on the three-dimensional morphology [12]. In the present study, the FPA-FTIRI spectroscopy was exploited to perform a

* Corresponding author.
*E-mail address:* v.notarstefano@univpm.it (V. Notarstefano).

http://doi.org/10.1016/j.clispe.2021.100011
Received 21 December 2020; Received in revised form 15 March 2021; Accepted 23 May 2021

hyperspectral imaging analysis on a spheroid model obtained by the MSTO-211H cell line (deriving from biphasic lung mesothelioma), with the aim to: (1) evaluate differences in the macromolecular features of cells in relation with their position within spheroid models, and (2) obtain new insights on the effects induced by cisplatin treatment.

## Materials and methods

### *Cell culture and drugs treatment*

According to Zanellato et al., MSTO-211H cells were seeded in U-shaped plates and incubated on an orbital mixer in a standard incubator, letting obtain, after 4 days, spheroids of 400−500 μm diameter [13,14]. N.2 MSTO-211H spheroids were treated for 72 h with cisplatin (1 μM) (**Cis**), while other N.2 spheroids, considered as control samples, were cultured under the same conditions without cisplatin (**Ctrl**). Then, all spheroid samples were washed in NaCl 0.9 % and frozen rapidly at −80 °C [15,16]. The experiment was performed in duplicate.

### *FPA-FTIRI measurements and data analysis*

FPA-FTIRI measurements were carried out at the SISSI Beamline, Elettra Sincrotrone Trieste (Trieste, Italy), using a Hyperion 3000 Vis–IR microscope coupled with a Vertex 70v interferometer and equipped with a Focal Plane Array (FPA) detector (164 x 164 μm; 4096 pixel/spectra; 2.56 μm spatial resolution) (Bruker Optics GmbH, Ettlingen, Germany). MSTO-211H spheroids were cut by a cryomicrotome to obtain 6 slides (8−10-μm-thick) for each sample. Four sections were deposited onto $CaF_2$ optical windows (1-mm thick, 13-mm diameter) and let air-dry for 30 min without any fixation process, for IR measurements [10], while the remaining slides were deposited onto glass slides, stained with Mayer's Hematoxylin and Eosin Y (Sigma-Aldrich, Milano, Italy) and analyzed by a Zeiss Axio Imager.A2 (Oberkochen, Germany) microscope equipped with a combined color digital camera Axiocam 503 (Zeiss).

On each unstained section, a multiple IR image, covering the spheroid diameter, was acquired in transmission mode (15X condenser/objective; 4000−900 $cm^{-1}$; 4 $cm^{-1}$ spectral resolution, and 256 scans). Background spectra were obtained on clean regions of the $CaF_2$ optical windows with the same acquisition parameters. Raw IR images were corrected with Atmospheric Compensation routine (OPUS 7.5 software, Bruker Optics GmbH, Ettlingen, Germany).

False color images were generated by integrating IR images in specific spectral regions, to evaluate the spatial distribution and the relative amount of: lipids (2995−2828 $cm^{-1}$, vibrational modes of lipid alkyl chains); proteins (1720−1480 $cm^{-1}$, Amide I and II bands, vibrational modes of peptide linkage), and nucleic acids/carbohydrates (1150−1000 $cm^{-1}$, vibrational modes of nucleic acids and carbohydrates).

Hierarchical Cluster Analysis (HCA) of the IR images was performed using the MATLAB toolbox IRootLab (https://github.com/trevisanj/irootlab) [17,18], by Euclidean distances and Ward's linkage method [19,20]. For each cluster identified by HCA, the average and average ± SD spectra were calculated (Averaging routine, OPUS 7.5), and curve fitted by using second derivative minima and Gaussian functions; the position and integrated areas of the underlying bands were identified (GRAMS/AI 9.1, Galactic Industries, Inc., Salem, New Hampshire).

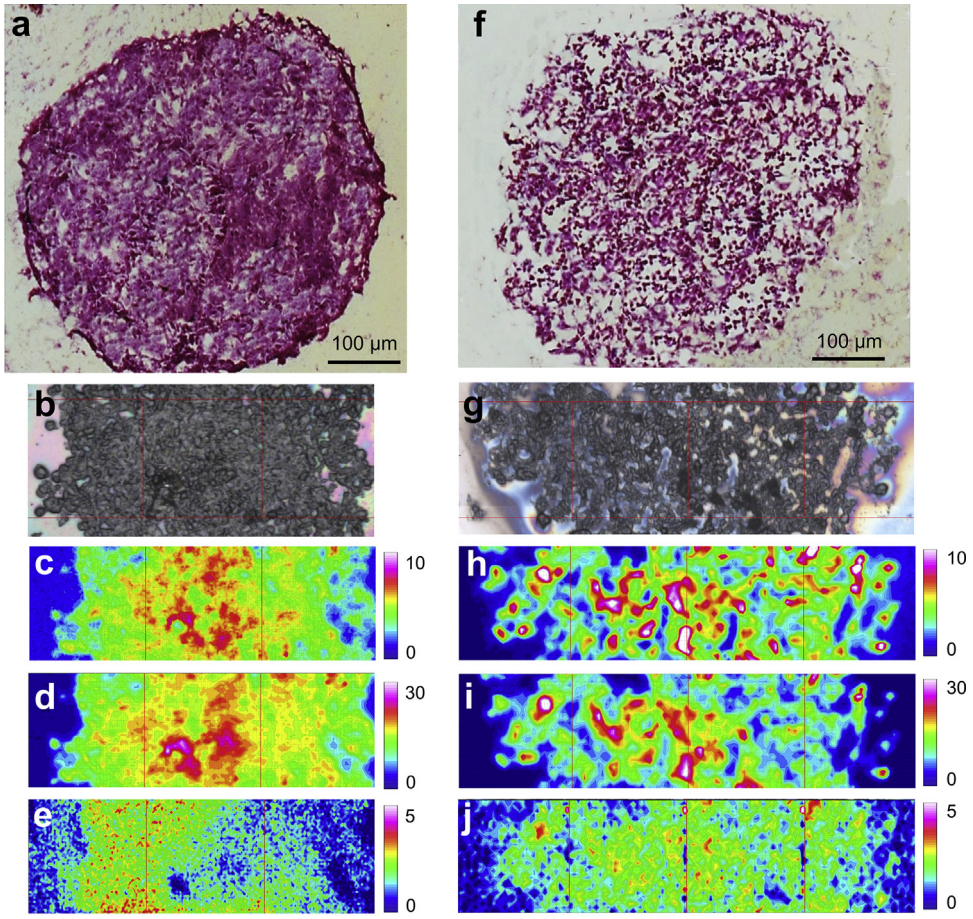


**Fig. 1.** Hyperspectral imaging analysis of MSTO-211H cell spheroids. Representative H&E sections of **Ctrl** (a) and **Cis** (f) samples. Microphotographs of **Ctrl** (b) and **Cis** (g) mapped areas. False color images showing the topographical distribution of lipids (c,h), proteins (d,i) and nucleic acids/carbohydrates (e,j) in **Ctrl** and **Cis** samples (different color scales were used for a better interpretation of the data).

## Results and discussion

The microphotographs of representative sections of H&E-stained **Ctrl** and **Cis** MSTO-211H spheroids are showed in Fig. 1, together with the microphotographs of the IR mapped areas and the corresponding IR false colour images representing the topographical distribution of lipids, proteins and nucleic acids/carbohydrates. The morphological analysis of H&E **Ctrl** sections of MSTO-211H spheroids evidenced the cellular network characterizing the architecture of these samples (Fig. 1a); moreover, the distribution of lipids (Fig. 1c), proteins (Fig. 1d) and nucleic acids/carbohydrates (Fig.1e) showed by IR false colour images, appeared consistent with the presence of a high proliferative outer region, rich in nucleic acids, and an inner hypoxic one, characterized by a major cellular density, as displayed by the major amount of lipids and proteins [4]. As regards **Cis** samples, a partial loss of structural integrity caused by the treatment was observed (Fig. 1g), as confirmed also by the homogeneous distribution in lipids (Fig. 1h), proteins (Fig.1i) and nucleic acids (Fig.1j) displayed by IR false colour images; moreover, the

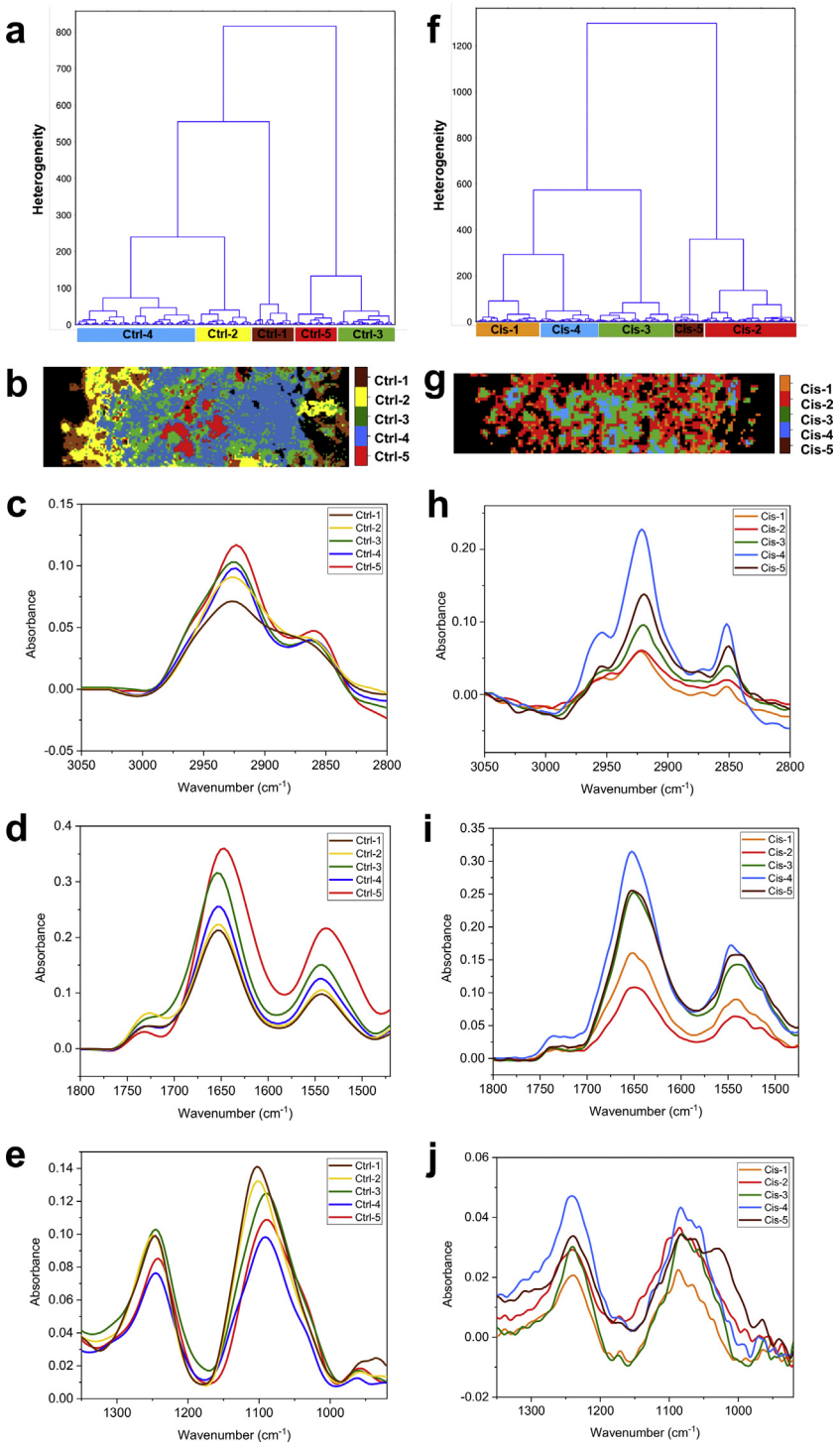


**Fig. 2.** Dendrograms obtained by Ward's algorithm and Euclidean distance measure criterion, displaying the five clusters highlighted in **Ctrl** (a) and **Cis** (f) samples and HCA spectroscopic images of **Ctrl** (b) and **Cis** (g) samples (**Ctrl-1** to **Ctrl-5**, and **Cis-1** to **Cis-5** clusters; black color indicates background spectra). Average spectra of **Ctrl** and **Cis** clusters in the following spectral ranges: 3050-2800 $cm^{-1}$ (c,h); 1800-1480 $cm^{-1}$ (d,i), and 1350-920 $cm^{-1}$ (e,j).

**Table 1**
Position, vibrational mode and biochemical assignment of the most relevant bands identified by curve fitting analysis of **Ctrl** and **Cis** average absorbance spectra.

| Wavenumbers (cm-1) | Vibrational mode and biochemical assignment | Refs. |
|---|---|---|
| ~2960, ~2925 | Asymmetric stretching vibrations of $CH_3$ and $CH_2$ groups in branched and linear lipid aliphatic chains | [10,16] |
| ~1740 | Stretching vibration of CO ester moieties in lipids | [21,22] |
| ~1650, ~1550 | Amide I and Amide II, vibrational modes of peptide linkage | [23] |
| ~1240, ~1220 | Asymmetric stretching vibrations of phosphate moieties of A and B- DNA | [16,24,25] |
| ~1085 | Symmetric stretching vibrations of phosphate moieties in nucleic acids | [26] |
| ~1054 | Stretching vibration of C−OH groups in carbohydrates | [27] |
| ~1020 | Stretching vibration of $CH_2$−OH groups in glycogen | [28] |

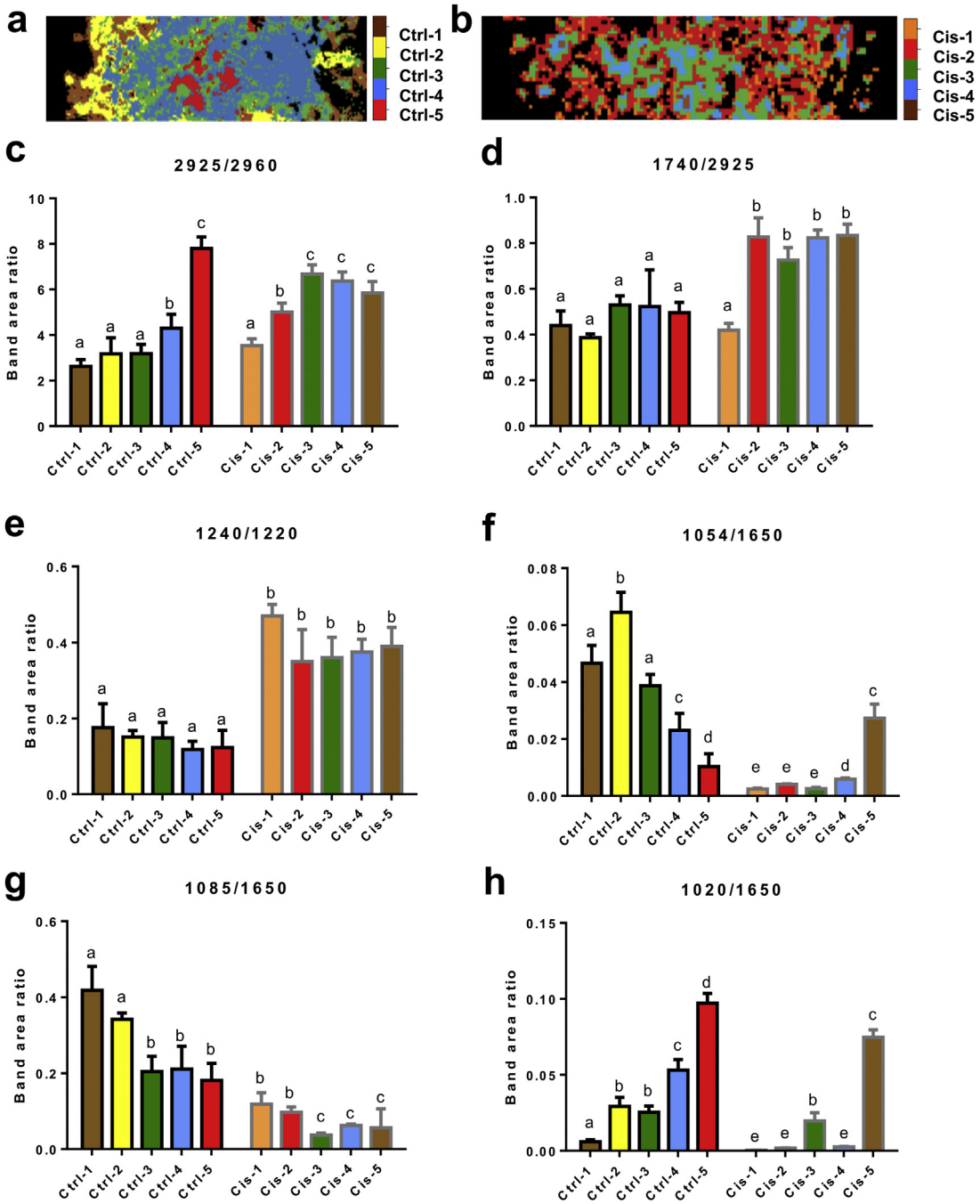


**Fig. 3.** HCA spectroscopic images of **Ctrl** (a) and **Cis** (b) samples. Statistical analysis of the following band area ratios calculated for **Ctrl** and **Cis** samples: (c) 2925/2960, (d)1740/2925, (e)1240/1220, (f) 1054/1650, (g) 1085/1650, and (h) 1020/1650. Data are presented as mean ± SD. Different letters over histograms indicate statistically significant differences among groups (one-way ANOVA and Tukey's multiple comparison test). Statistical significance was set at $p < 0.05$.

presence of some areas richer in lipids and proteins, is consistent with the known effect of cisplatin in tumour cells [15].

To better elucidate the different cellular features, IR maps were submitted to HCA analysis (Fig. 2): both in **Ctrl** and **Cis** samples, five clusters characterized by different spectral profiles were identified (Fig. 2a, f). As regards **Ctrl** sections, clusters (**Ctrl-1** to **Ctrl-5**) showed a concentric distribution, confirming the presence of different inner, intermediate and outer regions (Fig. 2b). In **Cis** samples, a clear correspondence between the HCA clusters' position (**Cis-1** to **Cis-5;** Fig. 2g) and the topographical distribution of proteins and lipids, observed within the IR false colour images, confirmed the loss of structural integrity. The average spectra of all HCA clusters were analyzed in the following regions of interest: 3050 −2800 $cm^{-1}$ (lipids, Fig. 2c,h), 1800−1480 $cm^{-1}$ (proteins, Fig. d,i), and 1350−920 $cm^{-1}$ (nucleic acids and carbohydrates, Fig. e,j). Both within **Ctrl** and **Cis** samples, visible differences were detected in band height and shape, confirming different environments between inner and outer regions. Moreover, **Ctrl** and **Cis** spectra showed significant differences between each other, as a result of the cisplatin action. In particular, as regards **Ctrl** samples, the five clusters mostly differed in the 3050−2800 $cm^{-1}$ (referred to the lipid component) and the 1350−920 $cm^{-1}$ (nucleic acids and carbohydrates) spectral ranges, both possibly ascribable to an altered metabolism of the inner spheroids' regions. Within **Cis** samples, more evident differences among clusters' spectral profiles were observed, letting hypothesize a penetration of cisplatin within the three-dimensional spheroid and the subsequent cellular damage.

The average and average ± SD spectra of each cluster identified by HCA were curve fitted (Table 1). Specific band area ratios were calculated and statistically analyzed (Fig. 3): (i) the statistically significant high values of the 2925/2960 band area ratio (length/branching of lipid aliphatic chains) found especially in **Ctrl-5** cluster, corresponding to the inner region, and in all **Cis** clusters (except for **Cis-1**, mostly located in the outer zone), is consistent with the known accumulation of lipid droplets in apoptotic cells (Fig.3c) [15]; (ii) the 1740/2925 band area ratio (lipid carbonyl esters) significantly increased in all **Cis** clusters, except for **Cis-1**, suggesting the occurrence of lipid peroxidation (Fig. 3d) [21,22]; (iii) the 1240/1220 band area ratio (A-*vs* B-DNA) significantly increased in all **Cis** clusters, consistently with the transition of B-DNA to the more disordered A-DNA due to intercalating agents treatments (Fig. 3e) [16,29,30]; (iv) accordingly, the decrease of the 1085/1650 band area ratio (nucleic acids) in all **Cis** clusters and in **Ctrl-3**, **Ctrl-4** and **Ctrl-5** ones suggested a fragmentation and rearrangement of DNA, related to apoptosis mechanisms (Fig. 3g) [15,16]; (v) the high levels of the 1054/1650 band area ratio in **Ctrl-1**, **Ctrl-2** and **Ctrl-3** clusters (outer spheroid regions) highlighted a region of more actively replicating cells [4], while the low values observed in **Cis** clusters may indicate the inhibition of cell division induced by cisplatin (Fig. 3f) [16]; (vi) the 1020/1650 band area ratio (glycogen) appeared significantly higher in the inner **Ctrl-4** and **Ctrl-5** clusters, accordingly with the known accumulation of glycogen in the inner hypoxic regions of spheroids [31], while the values near to zero found in almost all **Cis** clusters, except **Cis-5**, probably because of the loss of the spheroid structure (Fig. 3e)

## Conclusions

In the present study, FPA-FTIRI was exploited to elucidate the biochemical composition and the macromolecules distribution within the three-dimensional spheroid model obtained by the MSTO-211H cell line, and to assess the effects of cisplatin in terms of its penetrating ability into the core of the cell mass. The known organization of spheroids in an outer replicative region and an inner hypoxic and less proliferative one was confirmed, as evidenced by IR false colour images, HCA spectroscopic images, and band area ratios. The hyperspectral analysis showed that the changes in the spectral profile are indicative of alterations in specific biomolecules of crucial importance for the cell surviving. Cisplatin-treated samples displayed a partial loss of their three-dimensional structure, which let the drug penetrate and act on the majority of cells, and few differences were highlighted between inner and outer regions in terms of distribution and relative intensity of specific spectral features.

In conclusion, despite the limited number of included samples, this study represents a proof of concept of the high potential of FPA-FTIRI in providing a morpho-chemical correlation between histological and vibrational analysis, helping to gain a deeper understanding of the architecture of these three-dimensional spheroid models, by the biochemical composition analysis.

## Declaration of Competing Interest

The authors report no declarations of interest.

## Acknowledgments

The authors acknowledge Elettra Sincrotrone Trieste S.C.p.A. for accepting the Proposal N. 20177047 and providing beamtime to SISSI beamline experimental facility. The authors acknowledge Dr. Giulia Orilisi for providing support in statistical analysis. This work has been carried out within the HERMES project, "Progetto finanziato attraverso l'offerta di indennizzo ai residenti di Casale Monferrato deceduti o affetti da mesotelioma" (Project funded by offer of compensation to the residents of Casale Monferrato died or suffering from mesothelioma).

## References

[1] G. Mazzoleni, D. Di Lorenzo, N. Steimberg, Genes Nutr. 4 (2009) 13–22, doi:http://dx.doi.org/10.1007/s12263-008-0107-0.
[2] A. Ernst, S. Hofmann, R. Ahmadi, N. Becker, A. Korshunov, F. Engel, C. Hartmann, J. Felsberg, M. Sabel, H. Peterziel, M. Durchdewald, J. Hess, S. Barbus, B. Campos, A. Starzinski-Powitz, A. Unterberg, G. Reifenberger, P. Lichter, C. Herold-Mende, B. Radlwimmer, Clin. Cancer Res. 15 (2009) 6541–6550, doi:http://dx.doi.org/10.1158/1078-0432.CCR-09-0695.
[3] S.A. Langhans, Front. Pharmacol. 9 (2018) , doi:http://dx.doi.org/10.3389/fphar.2018.00006.
[4] J.Z. Zhang, N.S. Bryce, R. Siegele, E.A. Carter, D. Paterson, M.D. de Jonge, D.L. Howard, C.G. Ryan, T.W. Hambley, Integr. Biol. (Camb) 4 (2012) 1072–1080, doi:http://dx.doi.org/10.1039/c2ib20121f.
[5] J. Friedrich, R. Ebner, L.A. Kunz-Schughart, Int. J. Radiat. Biol. 83 (2007) 849–871, doi:http://dx.doi.org/10.1080/09553000701727531.
[6] C. Fischbach, R. Chen, T. Matsumoto, T. Schmelzle, J.S. Brugge, P.J. Polverini, D.J. Mooney, Nat. Methods 4 (2007) 855–860, doi:http://dx.doi.org/10.1038/nmeth1085.
[7] B. Desoize, Crit. Rev. Oncol. Hematol. 36 (2000) 193–207, doi:http://dx.doi.org/10.1016/S1040-8428(00)00086-X.
[8] S. Breslin, L. O'Driscoll, Oncotarget 7 (2016) 45745–45756, doi:http://dx.doi.org/10.18632/oncotarget.9935.
[9] A. Singh, N. Pruett, C.D. Hoang, Transl. Lung Cancer Res. 6 (2017) 248–258, doi:http://dx.doi.org/10.21037/tlcr.2017.04.12.
[10] V. Notarstefano, S. Sabbatini, C. Conti, M. Pisani, P. Astolfi, C. Pro, C. Rubini, L. Vaccari, E. Giorgini, J. Biophotonics (2019) 1–10, doi:http://dx.doi.org/10.1002/jbio.201960071.
[11] M. Api, V. Notarstefano, I. Olivotto, A. Cellerino, O. Carnevali, Zebrafish 15 (2018) 546–557, doi:http://dx.doi.org/10.1089/zeb.2018.1631.
[12] T. Srisongkram, N. Weerapreeyakul, K. Thumanu, Int. J. Mol. Sci. 21 (2020) 4141, doi:http://dx.doi.org/10.3390/ijms21114141.
[13] I. Zanellato, I. Bonarrigo, D. Colangelo, E. Gabano, M. Ravera, M. Alessio, D. Osella, J. Inorg. Biochem. 140 (2014) 219–227, doi:http://dx.doi.org/10.1016/j.jinorgbio.2014.07.018.
[14] I. Zanellato, D. Colangelo, D. Osella, Curr. Cancer Drug Targets 17 (2017) 1–13, doi:http://dx.doi.org/10.2174/1568009617666170623101722.
[15] E. Giorgini, S. Sabbatini, R. Rocchetti, V. Notarstefano, C. Rubini, C. Conti, G. Orilisi, E. Mitri, D.E. Bedolla, L. Vaccari, Analyst 143 (2018) 3317–3326, doi:http://dx.doi.org/10.1039/c8an00602d.
[16] V. Notarstefano, S. Sabbatini, C. Pro, A. Belloni, G. Orilisi, C. Rubini, H.J. Byrne, L. Vaccari, E. Giorgini, Analyst (2020) , doi:http://dx.doi.org/10.1039/D0AN01623C.
[17] J. Trevisan, P.P. Angelov, A.D. Scott, P.L. Carmichael, F.L. Martin, Bioinformatics 29 (2013) 1095–1097, doi:http://dx.doi.org/10.1093/bioinformatics/btt084.
[18] F.L. Martin, J.G. Kelly, V. Llabjani, P.L. Martin-Hirsch, I.I. Patel, J. Trevisan, N.J. Fullwood, M.J. Walsh, Nat. Protoc. 5 (2010) 1748–1760, doi:http://dx.doi.org/10.1038/nprot.2010.133.
[19] B. Bird, M. Miljkovic, M.J. Romeo, J. Smith, N. Stone, M.W. George, M. Diem, BMC Clin. Pathol. 8 (2008) , doi:http://dx.doi.org/10.1186/1472-6890-8-8.
[20] M.J. Baker, J. Trevisan, P. Bassan, R. Bhargava, H.J. Butler, K.M. Dorling, P.R. Fielden, S.W. Fogarty, N.J. Fullwood, K.A. Heys, C. Hughes, P. Lasch, P.L. Martin-Hirsch, B. Obinaju, G.D. Sockalingum, J. Sulé-Suso, R.J. Strong, M.J. Walsh, B.R. Wood, P.

Gardner, F.L. Martin, Nat. Protoc. 9 (2014) 1771–1791, doi:http://dx.doi.org/10.1038/nprot.2014.110.
[21] G. Gioacchini, V. Notarstefano, E. Sereni, C. Zacà, G. Coticchio, E. Giorgini, L. Vaccari, O. Carnevali, A. Borini, MHR Basic Sci. Reprod. Med. 24 (2018) 521–532, doi:http://dx.doi.org/10.1093/molehr/gay035.
[22] V. Notarstefano, G. Gioacchini, H.J. Byrne, C. Zacà, E. Sereni, L. Vaccari, A. Borini, O. Carnevali, E. Giorgini, Spectrochim. Acta Part A Mol. Biomol. Spectrosc. 212 (2019) 206–214, doi:http://dx.doi.org/10.1016/j.saa.2018.12.054.
[23] M.J. Baker, E. Gazi, M.D. Brown, J.H. Shanks, N.W. Clarke, P. Gardner, J. Biophotonics 2 (2009) 104–113, doi:http://dx.doi.org/10.1002/jbio.200810062.
[24] D.R. Whelan, K.R. Bambery, P. Heraud, M.J. Tobin, M. Diem, D. McNaughton, B.R. Wood, Nucleic Acids Res. 39 (2011) 5439–5448, doi:http://dx.doi.org/10.1093/nar/gkr175.
[25] D. Ghosh, S.K. Dey, C. Saha, PLoS One 9 (2014) e84880, doi:http://dx.doi.org/10.1371/journal.pone.0084880.
[26] P. Zucchiatti, E. Mitri, S. Kenig, F. Billè, G. Kourousias, D.E. Bedolla, L. Vaccari, Anal. Chem. 88 (2016) 12090–12098, doi:http://dx.doi.org/10.1021/acs.analchem.6b02744.
[27] V. Notarstefano, G. Gioacchini, E. Giorgini, N. Montik, A. Ciavattini, A.R. Polidori, F.A. Candela, L. Vaccari, M. Cignitti, O. Carnevali, Int. J. Mol. Sci. 21 (2020) 7124, doi:http://dx.doi.org/10.3390/ijms21197124.
[28] A.C.S. Talari, M.A.G. Martinez, Z. Movasaghi, S. Rehman, I.U. Rehman, Appl. Spectrosc. Rev. 52 (2017) 456–506, doi:http://dx.doi.org/10.1080/05704928.2016.1230863.
[29] A. Mignolet, A. Derenne, M. Smolina, B.R. Wood, E. Goormaghtigh, Biochim. Biophys. Acta - Proteins Proteomics 1864 (2016) 85–101, doi:http://dx.doi.org/10.1016/j.bbapap.2015.08.010.
[30] J.L. Denbigh, D. Perez-Guaita, R.R. Vernooij, M.J. Tobin, K.R. Bambery, Y. Xu, A.D. Southam, F.L. Khanim, M.T. Drayson, N.P. Lockyer, R. Goodacre, B.R. Wood, Sci. Rep. 7 (2017) 2649, doi:http://dx.doi.org/10.1038/s41598-017-02069-5.
[31] S. Riffle, R.N. Pandey, M. Albert, R.S. Hegde, BMC Cancer 17 (2017) 338, doi:http://dx.doi.org/10.1186/s12885-017-3319-0.